First-in-Human Clinical Trial of Vaccination with WDVAX, a Dendritic Cell–Activating Scaffold Incorporating Autologous Tumor Cell Lysate, in Patients with Metastatic Melanoma

F. Stephen Hodi[1,2,3,4], Anita Giobbie-Hurder[2,5], Kwasi Adu-Berchie[6], Srin Ranasinghe[2], Ana Lako[2], Mariano Severgnini[2], Emily M. Thrash[2], Jason L. Weirather[2,7], Joanna Baginska[2], Michael P. Manos[2,3], Edward J. Doherty[6,8], Alexander Stafford[6], Heather Daley[1,9], Jerome Ritz[1,9], Patrick A. Ott[1,3,4], Kathleen L. Pfaff[2], Scott J. Rodig[2,4,10], Charles H. Yoon[11], Glenn Dranoff[1], and David J. Mooney[6,12]

ABSTRACT

The optimal means to prime for effective antitumor immunity in a patient with cancer remain elusive in the current era of checkpoint blockade. Crafting a strategy to amplify the number and function of $CD8^+$ T cells while blocking regulatory cells should increase immunotherapy efficacy. Biomaterial carriers have been demonstrated in preclinical studies to amplify the effects of immunomodulatory agents, synergistically integrate the effects of different agents, and concentrate and manipulate immune cells *in vivo*. Herein, we report data from a phase I trial in patients with metastatic melanoma who received the cytokine GM-CSF and the innate Toll-like receptor 9 agonist CpG oligonucleotide admixed with autologous tumor lysate onto a microporous poly-lactide-co-glycolide matrix polymer scaffold that achieves precise control over the spatial and temporal release of immunostimulatory agents *in vivo*. This materials system (WDVAX) served as a physical antigen-presenting structure to which dendritic cells and other immune-stimulating cells are recruited and activated. In this first clinical trial of a macroscale biomaterial–based vaccine, WDVAX treatment was found to be feasible and to induce immune activation in patients with melanoma.

Introduction

Therapeutic cancer vaccines offer great potential for cancer immunotherapy, and various biomaterial carriers of antigens and adjuvants have been demonstrated to obviate delivery issues of typical cancer vaccine strategies (1–3). Although a number of nanoparticle approaches have been explored in cancer immunotherapy (3–8), there are also macroscale materials–based systems that can mimic immune reactions that occur during local infection (1, 2, 9–11). Following administration, these materials form a defined microenvironment with micro-sized pores capable of housing recruited immune cells, and both antigen and adjuvant can be locally released over various time scales (1, 2, 9, 11–13). Efficient lymph node homing of the resulting antigen-loaded, activated antigen-presenting cells has been demonstrated (9–11).

The cytokine GM-CSF possesses potential dual roles in tumor immunity. Although it can lead to the accumulation and proliferation of dendritic cells, the homeostatic function of GM-CSF maintains immune tolerance by supporting regulatory T cells (Treg) through the production of TGF-β, MHC class II, and CCL22 by dendritic cells. However, in the presence of a second signal (e.g., a ligand for a Toll-like receptor), this tolerance pathway is downregulated, and GM-CSF activity on dendritic cells switches toward immune stimulation, with the induction of Th1, Th17, and $CD8^+$ T cells (14–17). These results suggest that codelivery of GM-CSF with a Toll-like receptor agonist might lead to the activation of dendritic cells and sustained induction of cytotoxic T cells (an antitumor dendritic cell–directed immune response) while diminishing the protoleragenic generation of Tregs.

In this study, we have utilized a macroporous poly-lactide-co-glycolide (PLG) matrix polymer scaffold that allows precise control over the spatial and temporal release of the immunostimulatory agents GM-CSF and CpG oligonucleotides *in vivo* (9, 10). This macroscale materials system serves as a physical, antigen-presenting structure with a large surface area to which dendritic cells (and other immune elements) may be recruited and then activated. We have previously shown that subcutaneous implantation of the GM-CSF/CpG/melanoma cell lysate–containing scaffolds in mice resulted in the local recruitment of dendritic cell responses that persisted for 2 weeks and were associated with increasing levels of IL12, IFN-α, and IFN-γ and the regression of day 9 tumors in approximately half of the animals (10). PLG degrades by simple hydrolysis of ester bonds into lactic acid and glycolic acids, which are removed by normal metabolic pathways (9, 18, 19), and it is one of the few biodegradable polymers approved for human use by the FDA (20).

We hypothesized that this engineered scaffold cancer vaccine, which we termed WDVAX, can generate effective antitumor immunity

[1]Department of Medical Oncology, Dana-Farber Cancer Institute, Boston, Massachusetts. [2]Center for Immuno-Oncology, Dana-Farber Cancer Institute, Boston, Massachusetts. [3]Melanoma Disease Center, Dana-Farber Cancer Institute, Boston, Massachusetts. [4]Harvard Medical School, Boston, Massachusetts. [5]Division of Biostatistics, Department of Data Science, Dana-Farber Cancer Institute, Boston, Massachusetts. [6]Wyss Institute for Biologically Inspired Engineering at Harvard University, Boston, Massachusetts. [7]Department of Data Science, Dana-Farber Cancer Institute, Boston, Massachusetts. [8]Attivare Therapeutics Inc., Natick, Massachusetts. [9]Cell Manipulation Core Facility, Dana-Farber Cancer Institute, Boston, Massachusetts. [10]Department of Pathology, Brigham and Women's Hospital, Boston, Massachusetts. [11]Department of Surgery, Brigham and Women's Hospital, Boston, Massachusetts. [12]Harvard Paulson School of Engineering and Applied Sciences, Cambridge, Massachusetts.

Corresponding Author: F. Stephen Hodi, Department of Medical Oncology, Dana-Farber Cancer Institute, 450 Brookline Avenue, Boston, MA 02215. E-mail: stephen_hodi@dfci.harvard.edu

Cancer Immunol Res 2025;13:978–89

doi: 10.1158/2326-6066.CIR-24-0333

by optimizing tumor antigen presentation while limiting the generation of Tregs, resulting in a beneficial antitumor microenvironment of immune effector cells and cytokines. To test this hypothesis, we conducted a first-in-human trial of WDVAX in patients with metastatic melanoma.

Materials and Methods

Study design

In this phase I trial of WDVAX, participants with stage IV melanoma and surgically accessible metastases were evaluated in a dose-escalation design based on decreasing time intervals between scaffold implantations: cohort 1 at monthly intervals, cohort 2 at 3-week intervals, and cohort 3 at 2-week intervals. There were three cohorts of five participants each. If no grade 3 or higher toxicities related to scaffold implantation were observed, up to an additional 10 participants were planned at the highest dose level (maximum tolerated dose; shortest interval time) as an expansion cohort (Supplementary Fig. S1). The primary study objectives were to determine the feasibility of WDVAX for metastatic melanoma and to assess the safety and biological activity of WDVAX. The secondary objectives included overall survival and analysis of immune response.

Feasibility was assessed by the ability to make WDVAX from tumor samples in quantities sufficient for four vaccinations. We also aimed that the time between resection and the first vaccine treatment was not more than 28 days. The primary assessment of feasibility was based on the 15 participants enrolled in the dose-escalation cohorts. WDVAX therapy would be considered feasible if no more than 50% of participants had insufficient vaccine or began therapy more than 28 days after resection. Toxicities were reported using the Common Terminology Criteria for Adverse Events version 4.0. Each event type was classified according to the worst grade reported in a patient for that event.

The eligibility criteria for participants with stage IV melanoma included surgically accessible metastasis and a performance status of 0 to 1. All participants provided written informed consent prior to enrollment. The clinical study was approved and monitored by the Dana-Farber/Harvard Cancer Center Institutional Review Board (Clinicaltrials.gov: NCT01753089). Dana-Farber/Harvard Cancer Center is guided in its human subject research by the ethical principles set forth in the Belmont Report.

GM-CSF microsphere preparation

The microspheres were manufactured using a double emulsion process to encapsulate GM-CSF. GM-CSF (Leukine, sargramostim; recombinant GM-CSF-Yeast-Expressed; Sanofi), lyophilized 250 μg/vial (1.4×10^6 IU/vial) was obtained through the Dana-Farber Cancer Institute Pharmacy. Encapsulation within the poly-lactic-co-glycolic acid (PLGA) microsphere (Supplementary Fig. S2) was performed by Phosphorex, Inc. The first emulsion solution was prepared by dissolving PLGA (LakeShore Biomedical) in ethyl acetate (Sigma-Aldrich) while stirring. The second emulsion solution was prepared by adding 7% ethyl acetate and 1% polyvinyl alcohol (PVA; Sigma-Aldrich) to deionized water (Lonza Walkersville Inc.) and mixing for 10 minutes. Microspheres were rinsed in a solution made by adding 7% ethyl acetate and 0.3% PVA to deionized water and mixing thoroughly. Nine-hundred microliters of the first emulsion solution was added to a 2 mL siliconized glass tube. Using a pipette, 100 μL of a 130 μg GM-CSF solution was added to 900 μL of water. The solution was then exposed to sonication (Branson Ultrasonics) for 15 seconds at 60 AMPs to create spheres of the GM-CSF solution, which were then coated with the dissolved PLGA polymer. The second emulsion precipitated the polymer by reducing the solubility of the PLGA, creating a solid coating around the GM-CSF solution. The combination of the first and second emulsions was then quickly added to a 200 mL bath containing 7% ethyl acetate, 0.3% PVA, and deionized water. This final bath removed additional solvent from the microspheres, and the stirring motion served to separate the microspheres. The microspheres were allowed to stir for 3 hours, during which time the ethyl acetate evaporated from the baths, causing additional solvent to be extracted from the microspheres. After rinsing, the microspheres were filtered to separate them from the rinse bath. The spheres were rinsed in a container with deionized water, flash-frozen, and lyophilized. GM-CSF microspheres were tested for GM-CSF content by ELISA, particle size, sterility, and endotoxin prior to release and were then stored at −20°C until needed.

Condensation of oligonucleotide

To incorporate CpG oligonucleotide (Pfizer) into PLGA scaffolds, it must first be condensed with polyethylenimine (PEI; Sigma-Aldrich). Clinical-grade CpG (7909 Lot AQQ-06H-008) was obtained from Pfizer via PPD. The process used to prepare the condensed oligonucleotide began with a solution prepared by adding 15 mg of oligonucleotide to 50 mL of deionized water. A PEI working solution (4.3 mg/mL) was prepared and adjusted to a pH of 7.4. Sixty-three microliters of the PEI working solution was added to 1.937 mL of PBS and vortexed. To condense the oligonucleotide, 1 mL of the oligonucleotide solution was added dropwise to the PEI/PBS solution while vortexing. The condensed oligonucleotide solution was allowed to stand for 15 minutes, and then 60 μL of a 50% sucrose solution (Sigma-Aldrich) was added and vortexed. The sucrose was used to stabilize the oligonucleotide and served as a vehicle to handle the small amounts of condensed oligonucleotide. Each 2 mL preparation represented one device equivalent of oligonucleotide (300 μL). The condensed oligonucleotide solution was frozen in an −80°C freezer and then lyophilized. The condensed oligonucleotide was then stored at −20°C until use (Supplementary Fig. S3).

Uncondensed oligonucleotide assay

The oligonucleotide (CpG, Pfizer) used in the manufacturing process was condensed with PEI and then lyophilized in a PBS and sucrose solution (see "Condensation of oligonucleotide"). To conduct the uncondensed oligonucleotide assay, the oligonucleotide was dissolved in water for infusion. Serial dilutions were performed to achieve concentrations that were within the range of the assay. The fluorescent stain used in the assay binds to the nucleic acid in order to quantify content.

This assay was used to analyze unprocessed CpG samples. Oligonucleotide samples were quantified using the Quant-iT OliGreen ssDNA Reagent from Invitrogen. OliGreen is an ultrasensitive nucleic acid stain for quantifying oligonucleotides in solution. It is tenfold more sensitive than traditional quantitation by ultraviolet absorbance. Once bound to DNA, OliGreen fluoresces at a specific wavelength (excitation 480 nm; emission 520 nm). A standard curve ranging from 1.0 to 3.0 μg/mL was generated using a commercially purchased oligonucleotide standard. The oligonucleotide standard and test samples were diluted in parity to maintain matrix consistency between them. The OliGreen reagent containing the fluorescent stain was diluted 1:200 in PBS. One-hundred microliters of this

diluted reagent was added to 100 μL of the samples and standards in a black-bottom 96-well plate. The plate was mixed, and the fluorescence was measured using a plate reader set to an excitation of 480 nm and an emission of 520 nm. The unknown samples were quantified by comparison with the standard curve.

Condensed oligonucelotide assay

The oligonucleotide (CpG) used in the manufacturing process was condensed with PEI and then lyophilized in a PBS and sucrose solution (see "Condensation of oligonucleotide"). Oligonucleotide samples were quantified using the Quant-iT OliGreen ssDNA Reagent from Invitrogen. To conduct the assay, the condensed, lyophilized oligonucleotide was reconstituted in water. Serial dilutions were performed to achieve concentrations that were within the range of the assay. Heparin (Sigma-Aldrich; Cat. # H3149) was added to each of the samples to a final concentration of 32 ng/mL. The heparin disassociated the oligonucleotide from the PEI, allowing the fluorescent stain used in the assay to bind to the nucleic acid; the assay was conducted as per the uncondensed assay mentioned above.

GM-CSF microspheres and final scaffold assay

The GM-CSF (Leukine) used in the manufacturing process was encapsulated in PLGA microspheres, which then underwent CO_2 foaming prior to incorporation into the final scaffold product. To conduct the GM-CSF ELISA, the microspheres or scaffolds were extracted in glacial acetic acid overnight. The samples were then mixed with methylene chloride and then with PBS. Serial dilutions were performed to achieve concentrations that were within the range of the assay. Standard (Leukine) preparation was performed in parity with samples with the omission of methylene chloride to establish a standard curve range from 100 to 500 pg/mL. The unknown samples were quantified by comparison with the standard curve.

This assay was used to analyze in-process and product release samples. Samples assayed for GM-CSF concentration were quantified using a commercially available ELISA kit from R&D Systems, Inc. This assay uses the quantitative sandwich enzyme immunoassay technique. A mAb specific for GM-CSF has been precoated onto a microplate. Standards and samples were diluted in parity in order to maintain sample matrix consistency and were subsequently pipetted into the wells, where any GM-CSF present was bound by the immobilized antibody. After washing away any unbound substances, an enzyme-linked antibody specific for GM-CSF was added to the wells. Following a wash to remove any unbound antibody–enzyme reagent, a substrate solution was added to the wells, and color developed in proportion to the amount of GM-CSF bound in the initial step. The color development was stopped, and the intensity of the color was measured at 450 nm. This assay recognizes both natural and recombinant human GM-CSF.

Final scaffold oligonucleotide assay

The CpG content in final scaffolds was assayed using a commercial fluorescence ssDNA-binding assay. To conduct the assay, the final scaffolds were extracted overnight at 37°C in 3 mL of a 0.32 mg/mL heparin solution. The heparin disassociates the oligonucleotide from the PEI, allowing the fluorescent stain used in the assay to bind to the nucleic acid. Extraction samples were subsequently processed using a commercial nucleotide removal kit in order to isolate the CpG from the tumor lysate.

This assay was used to analyze final scaffold samples. Oligonucleotide samples were quantified using the Quant-iT OliGreen ssDNA Reagent from Invitrogen. OliGreen is an ultrasensitive nucleic acid stain for quantifying oligonucleotides in solution. It is tenfold more sensitive than traditional quantitation by ultraviolet absorbance. Once bound to DNA, OliGreen fluoresces at a specific wavelength (excitation 480 nm; emission 520 nm). A standard curve ranging from 0.6 to 5.0 μg/mL was generated using an in-house oligonucleotide standard. The oligonucleotide standard was prepared using a dilution matrix in parity with that of the samples. The OliGreen reagent, containing the fluorescent stain, was diluted 1:200 in PBS. One-hundred microliters of this diluted reagent was added to 100 μL of the samples and standards in a black-bottom 96-well plate. The plate was mixed, and the fluorescence was measured using a plate reader set to an excitation of 480 nm and an emission of 520 nm. The unknown samples were quantified by comparison with the standard curve.

Scaffold preparation in GMP facility

Melanoma tumor biopsies from the patients enrolled in the trial were collected at Brigham and Women's Hospital and transported to the Cell Manipulation Core Facility at Dana-Farber Cancer Institute, Boston. A sample was taken for sterility testing, and tissue was placed in medium with gentamicin and maintained at 4°C overnight. Tumor digestion was initiated the following morning, with the biopsy cut into small pieces in a biological safety cabinet using scalpels and forceps. A single-cell suspension was then created by enzymatic digestion with collagenase in a sterile bag in a stomacher. After digestion, cells were washed and counted. For the first 18 patients, RBCs were removed via Ficoll density centrifugation. It was subsequently deemed that RBC removal was no longer required. If insufficient cells were recovered, the tumor cell suspension was placed into short-term culture for expansion. The minimum number of cells required to begin the manufacturing of tumor lysate was 1.3×10^6 cells. If less than 1.3×10^6 cells were recovered, the cells could be placed into short-term culture for expansion. The medium for short-term culture was DMEM (Gibco), 10% FBS (HyClone), and gentamicin (final concentration 50 μg/mL). Adherent cell culture was initiated in tissue culture plates or tissue culture dishes. Cells were observed every 2 to 3 days. If >80% confluent, the cells were trypsinized (trypsin 0.9% EDTA, Gibco) and counted. If the minimum cell number was reached, lysate manufacture could begin. If the minimum cell number was not reached, the cells were placed back into culture. If confluence was <80%, a media change was performed. Tumor cell lysate was prepared from the digested or cultured tumor cell suspensions by four freeze-thaws in liquid N_2. Lysate was stored at ≤ −30°C until scaffold manufacture was initiated.

To prepare lysate-coated microspheres, lysate was thawed at ambient temperature. Lyophilized GM-CSF (0.180 g) was added to the lysate and vortexed. The vortexed lysate/microspheres were then submerged in liquid N_2 for 15 to 20 minutes, and the frozen mixture was lyophilized for approximately 96 hours. Lysate-coated microspheres were stored at −30°C or processed directly for final scaffold manufacture.

To prepare the final WDVAX scaffold, lysate-coated microspheres and oligonucleotide were thawed at ambient temperature, and the oligonucleotide (0.300–0.310 g) was added to the lysate-coated microspheres. Approximately 1.3 g of sucrose was added to the oligo-/lysate-coated microspheres and mixed very well with a sterile spatula. Individual scaffolds were made by weighing out

0.175 ± 0.005 g into a tablet press and pressed for 1 minute at 1,500 psi. Tablets were then placed in a pressure vessel for CO_2 foaming at approximately 800 psi for approximately 16 hours. Ten tablets/scaffolds were made for each patient and placed into individual sterile vials and stored at ≤ −80°C. For each patient, five scaffolds were used for testing. Three were used for release testing, and two were used for measurement of GM-CSF and oligo content (nonrelease). Five scaffolds were reserved for patient administration (four doses and one backup).

Final scaffold total protein

The melanoma tumor lysate in the final scaffolds was assayed using a commercial bicinchoninic acid (BCA) protein assay. Sample serial dilutions were performed in 0.1 N sodium hydroxide to achieve concentrations that were within the range of the assay. The BCA protein reagent used in the assay binds to proteins through copper (IV) complexes to quantify content.

This assay was used to determine the total protein in the final scaffold samples. Scaffold samples were quantified using the BCA protein assay from Thermo Electron. BCA is a sensitive protein assay for quantifying protein in solution. Scaffold samples were extracted in 0.1 N sodium hydroxide. A standard curve ranging from 100 to 400 μg/mL was generated using a commercially purchased melanoma cell lysate standard. The lysate standard and samples were serially diluted in 0.1 N sodium hydroxide in order to maintain matrix consistency between them. The BCA working reagent was prepared by combining 25 parts reagent A, 23 parts reagent B, and 2 parts reagent C. One-hundred microliters of the BCA working reagent was added to 100 μL of the sample and standards in a 96-well plate. The unknown samples were quantified by comparison with the standard curve.

Release criteria and preparation of the final product for implantation

Each scaffold was required to have the equivalent of 1×10^5 to 1×10^7 viable cells/scaffold. If melanoma cells were cultured prior to preparation, the lysate was required to be negative for *Mycoplasma* by qPCR. If cell culture was performed, *Mycoplasma* testing was performed by Labs, Inc. (now Eurofins VRL). Testing was conducted using the MycoSEQ test kit. Fourteen-day sterility testing was conducted in the Cell Manipulation Core Facility using the BACT Alert System. Two scaffolds were tested for bacterial and fungal sterility by direct inoculation and were required to be negative after 14 days of incubation. On the day of implantation, the WDVAX scaffold was removed from the freezer and incubated with 10 mL of sterile water for injection. After 3 hours of incubation, 9.5 mL of leached water for injection was removed and tested for endotoxin and Gram stain. Endotoxin testing was performed in the Cell Manipulation Core Facility using the Endosafe PTS system. Gram stain was performed at Brigham and Women's Hospital Microbiology Lab. The scaffold was kept in the remaining 0.5 mL of sterile water until Gram stain and endotoxin results were available. If the two remaining release tests were negative, the scaffold was brought to the procedure room for surgical implantation.

Scaffold toughness and modulus determination

The moduli and mechanical toughness of vaccines were determined via three-point bend testing using a texture analyzer (TA.XT Plus, Texture Technologies Corp.). Scaffold dimensions were accurately measured using a micrometer prior to compression testing (probe: HDP/3PB). The scaffold was placed on a three-point stage with quantification conducted under compression test mode (strain target = 5%, test speed = 0.6 mm/minute, post speed = 1.8 mm/minute, and trigger force = 2.0 g).

Immunostaining

All biopsy samples at the time points indicated in the text were formalin-fixed and paraffin-embedded according to standard histopathology protocols. "Pre" biopsies were collected prior to WDVAX administration, whereas "Post" biopsies were collected after WDVAX administration. Chromogenic IHC and multiplexed immunofluorescence (IF) were performed by staining 4-mm-thick formalin-fixed, paraffin-embedded whole-tissue sections with standard primary antibodies (Supplementary Table S1) per published protocols (21, 22). IF-stained slides were imaged with a PerkinElmer/Akoya Mantra microscope, and images were analyzed and quantified using inForm software (Akoya) per standard protocols (21, 22).

Soluble biomarker detection

Paired patient plasma samples from "pre" and "post" administration of WDVAX were thawed from storage in a −80°C freezer and immediately assayed for the detection of MIP1α, Ip10, IL1β, IL2, IL4, IL5, IL2R, IL6, IL7, IL8, IL10, IL12p70, IL13, IL17α, IL1RA, GCSF, IFNγ, GMCSF, TNFα, MIP1β, MCP1, TNFβ, ENA78, IL1a, IL15, MCP3, IL3, CD40L, and VEGFA using a custom ProcartaPlex Immunoassays (Thermo Fisher Scientific). Samples were tested in duplicate according to the manufacturer's protocol and measured using the Luminex FLEXMAP 3D System (Luminex Corporation). Markers were quantified by standard curve extrapolation. Changes over time were statistically analyzed using the longitudinal mixed modeling of the $\log_2$ transform of the fold change in concentration relative to pretreatment.

CyTOF

Peripheral blood mononuclear cells (PBMC) collected at three time points (pre: pretreatment; post 1: after the second implant; and post 2: after the fourth implant) were analyzed by cytometry by time of flight (CyTOF) as previously described (23). Briefly, PBMCs were thawed, washed, stained with two optimized antibody panels (Supplementary Table S2), and run on a Helios mass cytometer (Fluidigm), with a reference sample spike-in to control for batch effects (24). Data in the form of .fcs files were normalized, concatenated, and debarcoded before analysis. Population frequencies were determined by manual gating in FlowJo (FlowJo LLC, version 10.6).

Unsupervised analysis of patient immune profiles

Preprocessing

Single-cell CyTOF intensities from each patient were imported into R version 4.0.5. Outliers, defined as cells with any channel value outside five SDs from the mean in either direction, were filtered out. The cells from each patient were then annotated with the patient identification (ID) and other clinical and vaccine formulation information, after which they were down-sampled to keep the same number of cells per patient. Fully annotated, down-sampled cells from all patients were pooled together for downstream analyses.

Dimensionality reduction

Dimensionality reduction was performed using the Uniform Manifold Approximation and Projection for Dimension Reduction

(UMAP) package version 0.2.7 (25). UMAPs were plotted as scatter plots using ggplot2 version 3.3.3 (26) and annotated with the various marker intensities.

K-means

K-means was performed independently on the pooled, preprocessed cells without first performing dimensionality reduction. First, an elbow plot was generated to determine the optimum number of clusters (K) by estimating the total within the sum of squares iterated from K = 1 to 15. The optimum K was estimated as the point at which increasing K does not substantially decrease the total within the sum of the squares of Euclidean distances between cells and K-cluster centroids. K-means clustering was then performed on the cells using the optimum number of clusters, after which the cluster assigned to each cell was overlaid onto the independently generated UMAP scatter plot to show concordance. The phenotypic markers that characterize a specific cluster (i.e., cluster centers) were then estimated by calculating the mean expression of each marker in each cluster and representing them as heatmaps using the pheatmap package version 1.0.12 (27). Clusters were assigned labels according to their phenotypes by expert review, and cell-type cluster frequencies were calculated for each patient.

Estimating trends of immune populations across time points

First, frequencies of cells in each cluster that belong to each patient at pre and either post 1 or post 2 time points were estimated. The frequencies were then split by patient ID, after which pairwise Euclidean distances were calculated per cluster for each patient between pre– and post 1– or post 2–time points, giving us the magnitude by which the immune profiles of each patient changed in the various clusters after treatment. The directions of change were defined as negative if, for a given patient, the frequency of cells in a cluster was higher at the pre–time point than at posttreatment, and *vice versa*. *P* values were determined by one-way ANOVA with repeated measures.

Data availability

The data generated in this study are available in the article, its supplementary files, and the Code Ocean capsule https://codeocean.com/capsule/3196830/tree/v1 or from the corresponding author upon request.

Results

Patients

Twenty-three patients were enrolled in three cohorts [cohort 1 (C1): $n = 5$, cohort 2 (C2): $n = 5$, and cohort 3 (C3; maximum tolerated dose): $n = 13$ (dose escalation: $n = 5$, dose expansion: $n = 8$)]. Patient characteristics are summarized in **Table 1**. All patients were White and non-Hispanic, and 57% were male. The median age at enrollment was 61 years (range: 42–85). Background information on melanoma and the representativeness of our study population is summarized in Supplementary Table S3. Approximately 70% (16 of 23) of patients reported prior therapy (including seven with prior anti–PD-1). Five of 23 patients had $BRAF^{V600E}$, and two harbored wild-type proteins. Ninety-six percent of patients (22 of 23) had Eastern Cooperative Oncology Group performance status = 0 (fully active). Among 21 patients who received at least one dose of vaccine (**Fig. 1**), the median follow-up was 21.1 months (inverted Kaplan–Meier).

Table 1. Demographic characteristics.

	All	
	N	**%**
Sex		
Female	10	43.5
Male	13	56.5
Age (years)		
Median (range)	61 (42–85)	
Race		
White	23	100.0
Ethnicity		
Non-Hispanic	23	100.0
Eastern Cooperative Oncology Group performance status		
0	22	95.7
1	1	4.3
Number of prior therapies		
0	7	30.4
1–2	12	52.2
3–5	4	17.4
Types of prior therapies (may have more than one)		
Immunotherapy	12	52.2
BRAF inhibitor	3	13.0
Kinase inhibitor	1	4.3
MEK inhibitor	1	4.3
Radiation	3	13.0
Chemoradiation	1	4.3
Radiosurgery	1	4.3
Chemotherapy	1	4.3
GVAX	1	4.3
Temozolomide	1	4.3
BRAF mutation		
No	12	52.2
Yes	7	30.4
Not done	4	17.4
Site of disease		
Extremities	6	25.8
Trunk	5	21.6
Eyes	1	4.3
Head and neck	2	8.6
Lobe, left lower	1	4.3
Lymph nodes, axillary	2	8.7
Skin	2	8.7
Testicle	1	4.3
Unknown	3	13.0

Feasibility

WDVAX was prepared in sufficient quantity for all but 1 of the 23 patients enrolled in the trial. All 15 participants in the three dose-escalation cohorts had their vaccines manufactured successfully, with a median of 10 vaccines manufactured per participant (range: 5–10) that satisfied the release criteria. One patient had disease progression prior to implantation. In the remaining 14 patients, the median number of days between tissue procurement and implantation of the first vaccine was 66 days (range: 29–116 days).

One of eight patients in the expansion cohort had insufficient tissue for vaccine production; five vaccines per patient were successfully produced for each of the remaining seven patients (Supplementary Fig. S1). The median number of days until the first implantation in this group was 35 days (range: 27–47 days). The vaccine implantation occurred in the outpatient setting via a small incision in the upper arms or thighs, followed by subcutaneous implantation of the device and subsequent closure with suture placement.

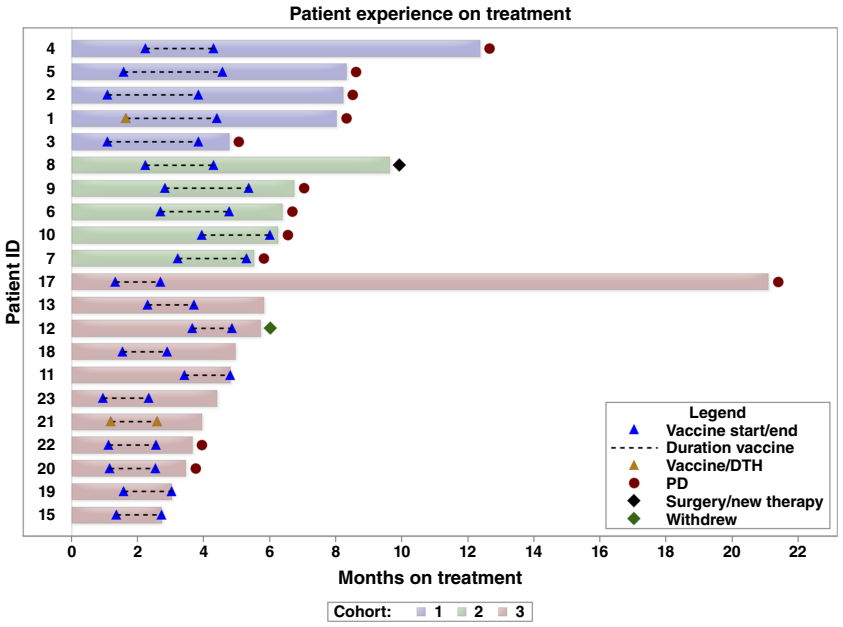

Figure 1.

Swimmer plot of patient experience on WDVAX. Swimmer plot of treatment duration and key clinical events for 21 patients treated with WDVAX. Each bar represents an individual patient, with the length corresponding to the duration of treatment. Symbols indicate key clinical events, such as duration of vaccine, disease progression, and change in participation status. Colors represent different dose-escalation cohorts, as detailed in the figure legend. Time on treatment is shown on the *x*-axis in months. Patients are ordered by time on treatment within the dose-escalation cohort. PD, progressive disease.

Vaccine characterization

Analysis of vaccines prepared for each of the enrolled patients generally confirmed the desired inclusion of GM-CSF, CpG oligonucleotides, and lysate prepared from the patients' tumors or tumor cells (collected from metastatic sites), which were culture-expanded to prepare the lysate. The average mass of vaccines was 26 ± 17 mg/scaffold (Supplementary Fig. S4A). The physical stability of the biomaterial vaccines was quantified by determination of compressive modulus and toughness, and median values were 430 and 2,300 Pa, respectively (Supplementary Fig. S4B and S4C), supporting the ability of the vaccines to remain intact during and after implantation. The mean GM-CSF content was 3.8 ± 2.0 μg, with mean CpG content of 89 ± 45 μg (Supplementary Fig. S4D and S4E). The cell equivalent of the lysate in each vaccine ranged from 0.1 to 10 million cells/scaffold (mean = 1.6 ± 2.6 million cells/scaffold; Supplementary Fig. S4F); the high variability was due to the varying tumor mass available for each patient. The average loading of bioactive agents was similar to those targeted in the vaccine design (3 μg GM-CSF, 100 μg CpG, 10^5–10^7 cell equivalents per scaffold).

Toxicities/adverse events

Nineteen of 21 vaccinated patients (90.5%) had one or more adverse events that were considered at least possibly related to the vaccine (Supplementary Table S4), including one case of grade 3 pneumonitis (cohort 3). There were no treatment-related grade 4 adverse events. The rate of treatment-related grade 3 to 4 adverse events was 4.8% [1 of 21, 90% confidence interval (CI), 0.2%–20.6%]. The most commonly occurring adverse events of all attributions were injection site reaction (16), hyperglycemia (9), and fatigue (Supplementary Table S5; ref. 8). No fatal adverse events occurred. The rate of grade 3 to 4 adverse events of all attributions among 21 treated patients was 23.8% (5 of 21; 90% CI, 9.9%–43.7%).

Survival of vaccinated patients

There were six deaths among 21 vaccinated patients (28.6%). All deaths were due to disease progression. There were no deaths in cohort 2. The median survival for the group as a whole was not reached; the 12-month survival estimate was 94% (90% CI, 72%–99%). There were 12 patients with disease progression (57.1%). The median time to progression (TTP) was 12.4 months (90% CI, 6.7–not reached); the 12-month TTP was 51% (90% CI, 28%–70%). The overall survival and TTP are presented in **Fig. 2**.

Best overall response

Best overall response (BOR) by cohort and overall for 21 vaccinated patients is summarized in Supplementary Table S6. Nine patients (42.9%; 90% CI, 24%–63%) had a BOR of stable disease, and 10 (47.6%) had a BOR of disease progression.

Vaccine and delayed-type hypersensitivity site reactions

Device-site reactions were recorded; among 21 patients who received the first vaccine, 18 reported erythema and 13 reported indurations. Representative local erythema at the site of WDVAX administration and histologic analyses are shown in **Fig. 3A–C**. Supplementary Table S7 summarizes induration and erythema (both in cm^2) by time point and cohort in patients reporting these reactions. Two patients, #1 and #21, had sufficient cells to test delayed-type hypersensitivity (DTH) with injections of lysate. Patient #1 had concurrent administration with vaccine #1, and patient #21 had DTH tested with vaccines #1 and #4.

Tumor immune microenvironment before and after vaccination

The quantification of melanoma ($SOX10^+$) and immune $PD\text{-}L1^+$ cells detected by multiplex IF (**Fig. 4A**) revealed a large range in the abundance of $SOX10^+PD\text{-}L1^+$ coexpressing cells across the pretreatment cohort (**Fig. 4E**). The quantitative analysis demonstrated high variability in immune cell population densities among the 15 patients with available pretreatment biopsies. In the patients with paired pre- and posttreatment biopsies, there was no clear change in $SOX10^+PD\text{-}L1^+$ cells by this analysis (**Fig. 4F**). T-cell and dendritic cell lineages were quantified by multiplex IF in tumor site biopsies from patients treated with WDVAX. T cells were identified using CD4 and CD8 (**Fig. 4B**, **C**, **G**, and **H**), whereas dendritic cells were

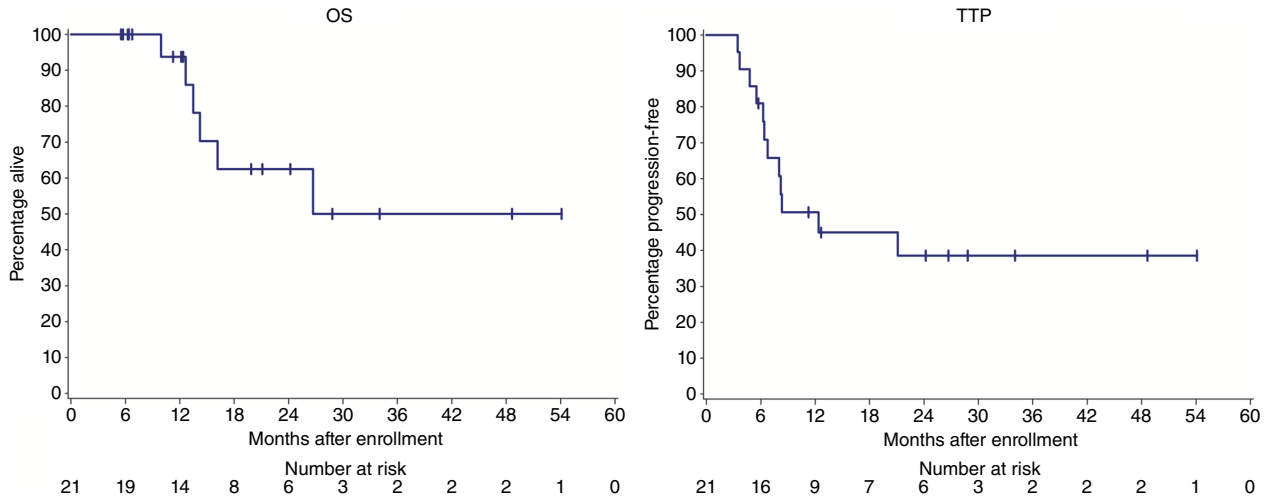

Figure 2.

Overall survival (OS) and TTP. Kaplan–Meier estimates of OS and TTP for 21 patients treated with WDVAX. The median OS was not reached. The 12- and 18-month OS estimates were 0.94 (90% CI, 0.72–0.99) and 0.63 (90% CI, 0.37–0.80), respectively. The median TTP was 12.4 months (90% CI, 6.7–not reached), and the 12- and 18-month estimates were 0.51 (90% CI, 0.28–0.70) and 0.45 (90% CI, 0.23–0.65), respectively. CIs are estimated using the log(−log) transformation method.

quantified using CD11c and CD68 (**Fig. 4D**, **I**, and **J**). There was a statistically significant increase in $CD4^+$ T-cell infiltration in five patients with matched pre- and posttreatment biopsies (**Fig. 4G**; Supplementary Fig. S5; $P = 0.03$), which is potentially indicative of their tissue-homing and helper role in orchestrating a wider immune response. Although two patients (patients #8 and #15) exhibited an increase in $CD8^+$ T-cell density, there was no clear trend in $CD8^+$ densities in these pre- and posttreatment samples (**Fig. 4H**; Supplementary Fig. S5; $P > 0.05$). Assessment of myeloid populations showed variability among patients, and none of the myeloid markers (CD68 or CD11c) showed a consistent trend between pre– and post 1– and post–2 time points (**Fig. 4D**, **I**, and **J**; Supplementary Fig. S5; $P > 0.05$). Assessment of these paired samples, although limited in number, implies varied biological action of the vaccine with heterogeneous induction of T cells and myeloid cells and lends support to the immunogenicity of the whole-lysate vaccine.

PBMCs were assigned to clusters according to their distinct immune cell phenotypes

To comprehensively characterize the systemic changes in the immune landscape induced by WDVAX in treated patients, we performed an in-depth, high-dimensional, single-cell analysis using mass cytometry. PBMCs were collected from patients across three time points: pre, post 1, and post 2. We analyzed changes in immune cell populations using a panel covering major immune lineages and markers (Supplementary Table S2) related to immune cell functions for innate and adaptive responses. K-means clustering identified 12 distinct immune populations (**Fig. 5A** and **B**; Supplementary Fig. S6). These populations included myeloid cells ($CD11b^+$), T cells ($CD3^+$), and NK cells ($CD56^+$; **Fig. 5C–E**). The analyzed cell clusters did not significantly change through the course of treatment (**Fig. 5F**).

Circulating soluble factors in response to vaccination

To understand the extent to which vaccination modulated the profiles of circulating chemokines, cytokines, and growth factors, Luminex analysis of matched plasma was performed for each patient pre- and posttreatment. Luminex detected 12 markers: IP10, IL4, IL2R, IL7, IL10, IL17A, MCP1, ENA78, MCP3, CD40L, IL1A, and VEGF-A. Of these, there were marginally significant increases in the concentrations of circulating VEGF-A and CD40L between pre– and post 2–time points (**Fig. 6**).

Discussion

Vaccinating patients with metastatic melanoma with a personalized dendritic cell–activating scaffold incorporating autologous

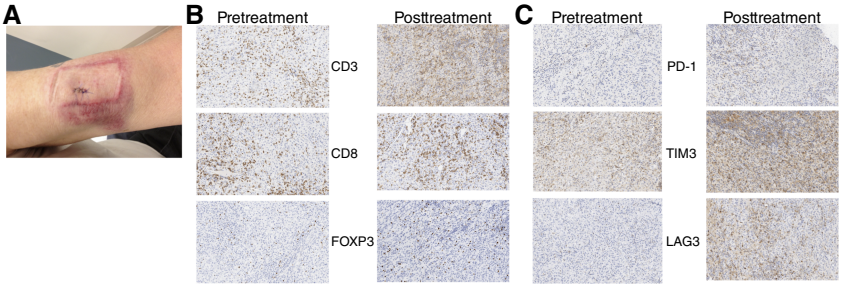

Figure 3.

Vaccine and delayed-type hypersensitivity site reactions. **A,** Photograph depicting local erythema in a representative patient at the site of WDVAX administration after treatment. **B** and **C**, Representative IHC staining for the indicated markers in a tissue biopsy taken prior to (pretreatment) or after WDVAX (posttreatment) showing (**B**) an increase in $CD3^+$, $CD8^+$, and $FOXP3^+$ immune cell populations and (**C**) an increase in the immune activation and exhaustion markers PD-1, TIM3, and LAG3.

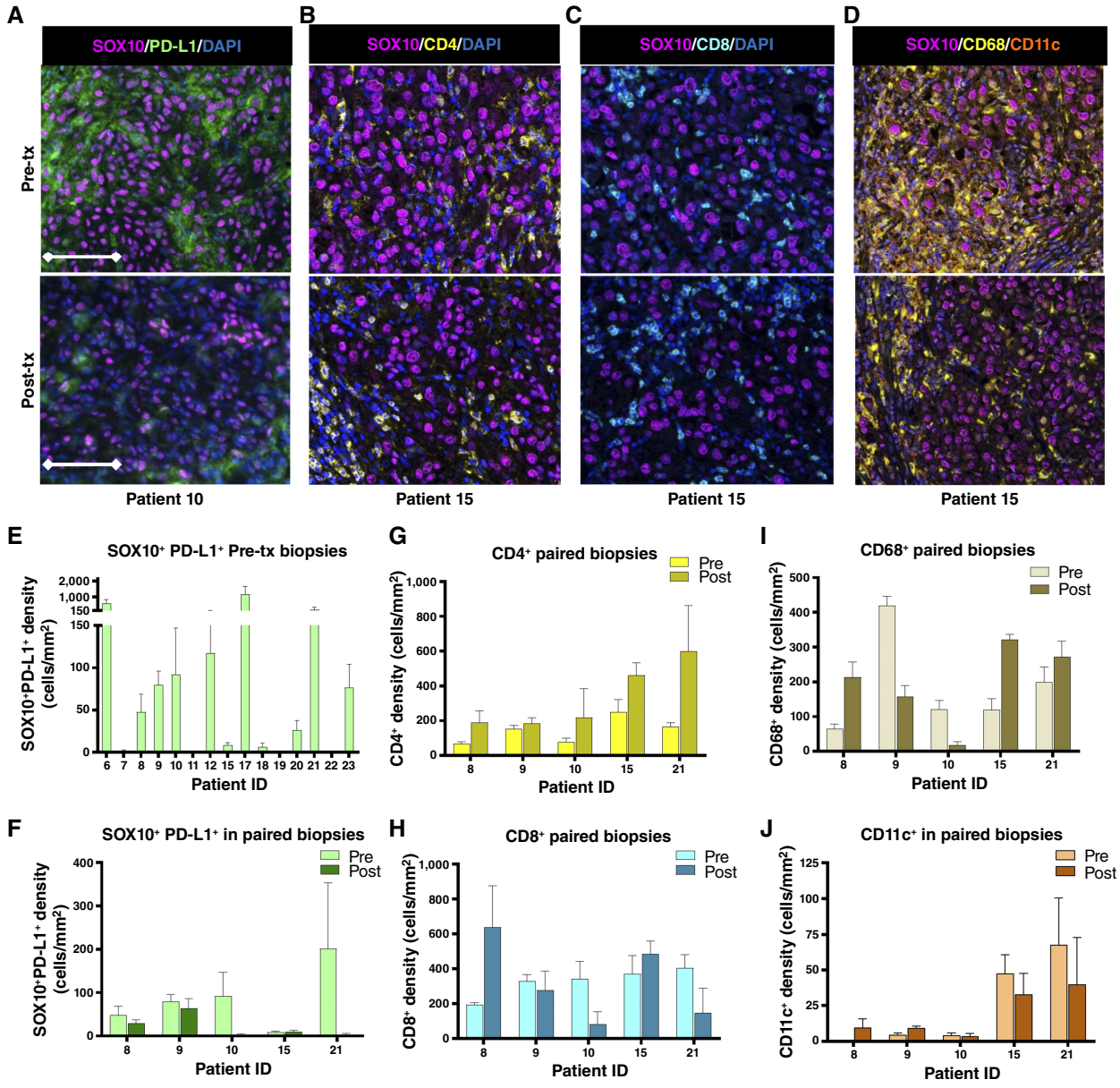

Figure 4.

Tumor-immune microenvironment before and after vaccination. **A–D,** Representative multiplex IF images from patients with paired pretreatment (top) and posttreatment (bottom) biopsies. Scale bar, 100 μm. **A,** SOX10 (magenta) and PD-L1 (green) in patient #10. **B,** CD4 (yellow) and SOX10 (magenta) in patient #15. **C,** CD8 (cyan) and SOX10 (magenta) in patient #15. **D**, CD68 (yellow), CD11c (orange), and SOX10 (magenta) in patient #15. In all images, nuclei are shown in blue with 4′,6-diamidino-2-phenylindole (DAPI). **E–J,** Quantification of cell densities (number of cells per mm^2 from multiplex IF staining). A minimum of three 20× regions of interest were quantified. Bar graphs represent the mean density across all regions of interest, and error bars represent SEM. **E,** $SOX10^+PD\text{-}L1^+$ coexpressing cells across all pretreatment samples. **F,** $SOX10^+PD\text{-}L1^+$ coexpressing cells in paired biopsies. **G,** $CD4^+$ Th cell densities in paired biopsies. **H,** $CD8^+$ cytotoxic T-cell densities in paired biopsies. **I,** $CD68^+$ macrophage densities in paired biopsies. **J,** CD11c dendritic cell densities in paired biopsies. Pre-tx, pretreatment; Post-tx, posttreatment.

cell lysate (WDVAX) proved feasible and safe in this first-in-human phase I trial. Most adverse events were low-grade and transient. One patient with grade 3 pneumonitis in cohort 3 may have experienced this as a result of nonspecific immune activation associated with the highest dose vaccine combined with the late effects of prior immune checkpoint blockade. Such toxicity can occur from immune checkpoint blockade and may potentially be delayed in onset. Further vaccine development strategies in combination with immune checkpoint blockade should take into consideration the possibility of such toxicity.

Clinical activity is difficult to assess in a selected patient population, requiring the ability to undergo surgery and time to

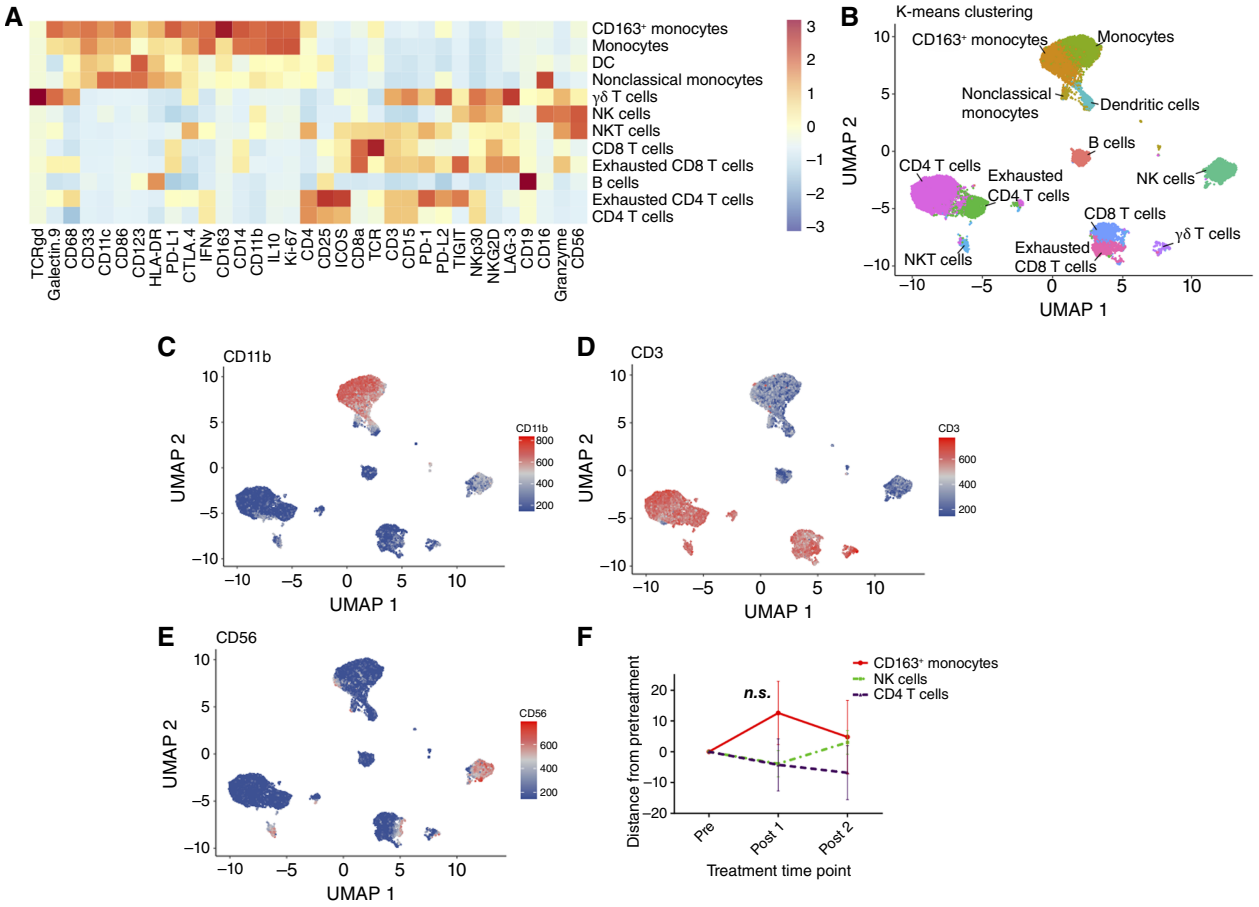

Figure 5.

Phenotypic analysis of immune cells harvested from patients at pre, post 1, and post 2 time points. PBMC populations from all patients at pre–, post 1–, and post 2–time points were pooled and analyzed. **A,** Marker expression within clustered cell populations indicates the annotation of distinct immune populations. UMAP of marker expression shows the panel distinguished. **B,** UMAP plot overlaid with K-means clustering of cell populations. **C,** CD11b$^+$ myeloid cells, (**D**) CD3$^+$ T cells, and (**E**) CD56$^+$ NK cells. **F,** Plot showing the changes in population frequencies for select clusters for post 1– and post 2–time points relative to the pre–time point. Data are mean ± SEM from $n = 20$ patients. *P* values were determined by one-way ANOVA with repeated measures. DC - dendritic cell; ns, not significant.

manufacture the vaccine. All patients had advanced melanoma with a small number classified as stage 4 no evidence of disease ($n = 6$), following surgical procurement of the tumor. Although approximately 43% of patients had stable disease as BOR by Response Evaluation Criteria in Solid Tumors (RECIST) criteria, the median survival and TTP may have exceeded expectations in this patient population. The potential impact of subsequent therapies on overall survival is not known. Overall, with a relatively small and selected patient population, the whole-cell vaccination strategy should be worthy of continued study.

The trial largely met the feasibility metrics established for the clinical trial. WDVAX was manufactured in the targeted quantities for 22 of the 23 enrolled patients. The scaffold dry weight was generally consistent between patients, except for the vaccine manufactured for patient #5, which exhibited a mass approximately fourfold larger than expected. The physical properties of the vaccines in the first patient cohort exhibited significant variability. This led us to reweigh components used in manufacturing (GM-CSF microspheres and PLG) and to initiate physical property testing of the vaccines manufactured for the remainder of the vaccines. The masses, moduli, and toughness were generally consistent for all subsequent vaccines. The GM-CSF and CpG content varied around the desired quantities but generally became more consistent with experience in manufacturing. There was significant variation in the lysate content of vaccines throughout the study because of the wide size variability of tumors harvested from each patient.

Despite the limitation of small patient numbers and variability in tumor size, there were apparent greater changes in immune activation as depicted in implant site pathology and peripheral blood analyses in cohorts in which vaccines were administered closer together in time. For clinical development, the timing of vaccinations provides important insight into both the rate of immune induction and the magnitude of antitumor immunity developed per treatment schedule with implications for potential combinations for efficacy and safety in the future.

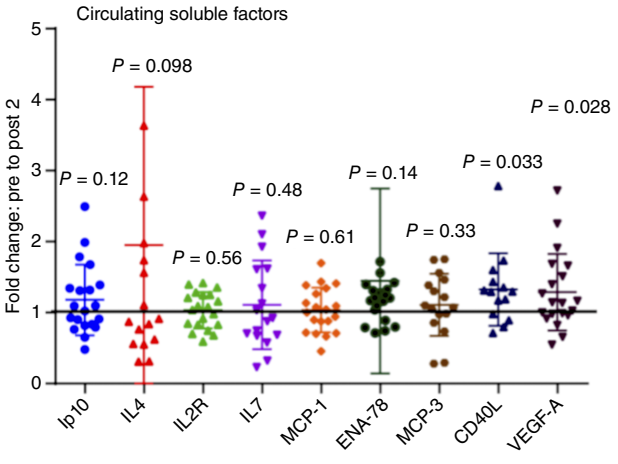

Figure 6.

Analysis of soluble factor secretion in response to vaccination. Fold change of the indicated circulating soluble factors from pre– to post 2–time point for each patient. The horizontal line indicates no change. Values > 1 show increased levels for a given patient from pre– to post 2–time point, and *vice versa*. Data are presented as mean ± SD for $n = 20$ patients. *P* values were calculated by performing a two-tailed *t* test.

Within the context of current cancer vaccine development, the source and type of antigens are key component parameters. In the current WDVAX study, whole-tumor cell lysate was utilized as an antigen. The advantage of such processing affords the opportunity to include multiple antigen classes, including neoantigens, cancer testis antigens, and melanosomal differentiation antigens. However, a limitation of our phase I study was that we could not interrogate the antigen in the tumor lysate or the tumor-specific T-cell responses that were primed. Further investigation is needed to better understand the relevant roles of these antigen types as well as whether there is a hierarchy in their induction of immune responses. The potential impact of an immune response to one class of antigen affecting that of another class will need rigorous investigation in patients in the future. In addition, combining this vaccination strategy with immune checkpoint blockade is needed to understand the combinatorial possibilities for priming the immune system with immune checkpoints. Both the relevant roles of antigen classes and the timing of the combination need to be explored clinically.

The findings of this clinical trial were partially consistent with previous studies utilizing subcutaneous implantation of the GM-CSF/CpG/melanoma cell lysate–containing WDVAX scaffold in murine models (9). Preclinical studies showed that WDVAX was well tolerated, without significant inflammatory or autoimmune toxicity, and these findings are consistent with the safety profile noted in this clinical trial. The preclinical studies also demonstrated local recruitment of a persistent DC infiltrate, robust levels of cytokines in the scaffolds consistent with the generation of Th1 responses, and the generation of antimelanoma $CD8^+$ T-cell responses both locally and systemically. The injection site reactions observed in most patients in this trial are consistent with the preclinical studies, whereas vaccine site enrichment with both dendritic cells and T cells in the clinical trial was inconsistent among patients. In a limited number of paired tissue samples, we observed that $CD4^+$ T cells increased to variable degrees in all five patients, whereas $CD8^+$ T-cell and myeloid cell infiltration were heterogeneous. There were too few cases to reach any definitive conclusions, but these data imply the vaccine was immunogenic in eliciting adaptive $CD4^+$ T cells and some innate immune responses. Immunophenotypic analyses of patients' PBMC populations, although not significant, showed heterogeneous responses following the WDVAX vaccine. As cytokines were not analyzed systemically in preclinical studies, it is unclear if the dynamics of cytokine levels observed in patients in the clinical trial are consistent with preclinical studies; the timing of sampling versus vaccination is also likely an important variable as the impact of vaccination on soluble cytokines is likely greatest in the days after vaccination. The soluble factor analyses may indicate functional relevance as GM-CSF is known to stimulate VEGF-A (28), and CD40 is required for the function of GM-CS–based whole-cell vaccination strategies (GVAX; ref. 29). In addition, MCP3 is known to recruit myeloid cells (30), whereas cytotoxic NK cells are associated with reduced VEGF-A, in contrast to NK cells that synthesize VEGF-A and contribute to tolerance. WDVAX, as monotherapy in the preclinical studies, mediated regression of B16F10 tumors in approximately half of the animals, whereas in the clinical study, 43% of patients treated with WDVAX exhibited stable disease. This clinical outcome may result from the finding that T cells in patients treated with WDVAX exhibited checkpoint markers that are inherently inhibitory and suggests amending future trials of WDVAX by using a second-generation vaccine in combination with checkpoint blockade.

In summary, this trial demonstrates the feasibility of this new type of biomaterial-based therapeutic vaccine. Vaccine was successfully manufactured for all patients, and the safety profile was favorable. The immune assessments, somewhat limited by sample availability, support immunogenicity of the vaccine although the expression of checkpoint markers in T cells in patients treated with WDVAX suggests combining future trials of WDVAX with checkpoint blockade. The median survival and TTP may have exceeded expectations in this patient population. Future modifications of WDVAX would preferably enable needle-based injection and allow for a further reduction in the time between tissue procurement and implantation.

Authors' Disclosures

F.S. Hodi reports nonfinancial support and other support from Pfizer during the conduct of the study as well as grants and personal fees from Bristol Myers Squibb; personal fees from Merck, Novartis, Compass Therapeutics, Apricity, Bicara Therapeutics, BioEntre, Gossamer, Rheos, Iovance Biotherapeutics, Bayer, Catalym, Immunocore, Kairos, Zumutor Biologics, Corner Therapeutics, Puretech, Curis, AstraZeneca, Pliant, Solu Therapeutics, Vir Biotechnology, 92Bio, and Checkpoint Therapeutics; and personal fees and nonfinancial support from Genentech outside the submitted work and has patents for Methods for treating MICA-related disorders (#20100111973); Angiopoiten-2 biomarkers predictive of anti-immune checkpoint response (#20170248603); Compositions and methods for identification, assessment, prevention, and treatment of melanoma using PD-L1 isoforms (#20160340407); Therapeutic peptides (#20160046716); Methods of using pembrolizumab and trebananib; Anti-galectin antibody biomarkers predictive of anti-immune checkpoint and anti-angiogenesis responses (publication number: 20170343552); and Antibodies against EDIL3 and methods of use thereof pending and patents for tumor antigens and uses thereof (#7250291), Therapeutic peptides (patent number: 9402905), Vaccine compositions and methods for restoring NKG2D pathway function against cancers (patent number: 10279021), and Antibodies that bind to MHC class I polypeptide–related sequence A (patent number: 10106611). A. Lako reports other support from Bristol Myers Squibb outside the submitted work. E.M. Thrash reports personal fees and other support from Standard BioTools and other support from Thermo Fisher Scientific, Olink, and Lunaphore Technologies outside the submitted work. J. Baginska reports personal fees from Compass Therapeutics outside the submitted work. E.J. Doherty reports he is a founder of a biotech company (Attivare Therapeutics Inc.) that has licensed some of the patents

for similar work. The general intellectual properties cited in this publication apply to Attivare's technology; however, the company is developing new intellectual property that utilizes alternative biomaterials, mechanisms, and indications. J. Ritz reports nonfinancial support from the Connell and O'Reilly Families Cell Manipulation Core Facility during the conduct of the study as well as grants from Kite/Gilead Sciences, Novartis, and Oncternal and personal fees from Akron Biotech, Astraveus, Garuda Therapeutics, Smart Immune, Tolerance Bio, TriArm Therapeutics, and TScan Therapeutics outside the submitted work. P.A. Ott reports grants and personal fees from Bristol Myers Squibb and Merck; grants from Celldex Therapeutics, Oncorus, Compass Therapeutics, Roche/Genentech, and Agenus; and personal fees from Imunon, PharmaJet, Phio, Servier, Arcturus, LG Chem, IO Biotech, and Innovent outside the submitted work. G. Dranoff reports other support from Novartis Pharmaceuticals outside the submitted work. D.J. Mooney reports nonfinancial support from Pfizer during the conduct of the study as well as grants and other support from Novartis; other support from Attivare Therapeutics, Medicenna, Lyell, Epoulosis, Limax Biosciences, Lighting Bio, Oddity Tech, Alkem, and Amend Surgical; and personal fees from ATCC, Johnson & Johnson, and Boston Scientific outside the submitted work and has patents for Scaffolds for cell transplantation and Mesoporous silica compositions for modulating immune responses, issued, licensed, and with royalties paid from Novartis, Attivare Therapeutics, and Lyell and patents for Controlled delivery of TLR agonists in structural polymeric devices, Injectable cryogel vaccine devices and methods of use thereof, Continuous cell programming devices, and Mesoporous silica compositions comprising inflammatory cytokines for modulating immune responses issued, licensed, and with royalties paid from Novartis and Attivare Therapeutics. No disclosures were reported by the other authors.

Authors' Contributions

F.S. Hodi: Conceptualization, resources, supervision, writing–original draft, writing–review and editing. **A. Giobbie-Hurder:** Data curation, formal analysis, writing–original draft, writing–review and editing. **K. Adu-Berchie:** Formal analysis, methodology. **S. Ranasinghe:** Supervision, writing–original draft, project administration. **A. Lako:** Formal analysis, methodology. **M. Severgnini:** Formal analysis, methodology. **E.M. Thrash:** Formal analysis, methodology. **J.L. Weirather:** Formal analysis, methodology, writing–review and editing. **J. Baginska:** Investigation. **M.P. Manos:** Data curation, project administration. **E.J. Doherty:** Conceptualization, investigation, methodology. **A. Stafford:** Formal analysis, investigation, methodology. **H. Daley:** Formal analysis, methodology. **J. Ritz:** Formal analysis, investigation, methodology. **P.A. Ott:** Investigation, writing–review and editing. **K.L. Pfaff:** Formal analysis, methodology. **S.J. Rodig:** Supervision, writing–original draft, writing–review and editing. **C.H. Yoon:** Resources, investigation. **G. Dranoff:** Conceptualization, supervision, investigation, writing–review and editing. **D.J. Mooney:** Conceptualization, resources, investigation, writing–original draft.

Acknowledgments

We thank all patients participating in the WDVAX phase I clinical trial and all members of the vaccine study team and surgical team, including Sara E. Russell, MD, and Jean Landry, NP. The trial was supported by research grant funding from Pfizer (WS2336880), the Sharon Crowley Martin Memorial Fund for Melanoma Research, the Malcolm and Emily MacNaught Fund for Melanoma Research, and the E. Michael Egan Melanoma Research Fund.

Note

Supplementary data for this article are available at Cancer Immunology Research Online (http://cancerimmunolres.aacrjournals.org/).

Received April 12, 2024; revised October 29, 2024; accepted April 10, 2025; posted first April 11, 2025.

References

1. Dellacherie MO, Seo BR, Mooney DJ. Macroscale biomaterials strategies for local immunomodulation. Nat Rev Mater 2019;4:379–97.
2. Adu-Berchie K, Mooney DJ. Biomaterials as local niches for immunomodulation. Acc Chem Res 2020;53:1749–60.
3. Irvine DJ, Hanson MC, Rakhra K, Tokatlian T. Synthetic nanoparticles for vaccines and immunotherapy. Chem Rev 2015;115:11109–46.
4. Yadav HKS, Dibi M, Mohammad A, Srouji AE. Nanovaccines formulation and applications-a review. J Drug Deliv Sci Technol 2018;44:380–7.
5. Nandedkar TD. Nanovaccines: recent developments in vaccination. J Biosci 2009;34:995–1003.
6. De Jong WH, Hagens WI, Krystek P, Burger MC, Sips AJAM, Geertsma RE. Particle size-dependent organ distribution of gold nanoparticles after intravenous administration. Biomaterials 2008;29:1912–9.
7. Kranz LM, Diken M, Haas H, Kreiter S, Loquai C, Reuter KC, et al. Systemic RNA delivery to dendritic cells exploits antiviral defence for cancer immunotherapy. Nature 2016;534:396–401.
8. Sindhwani S, Syed AM, Ngai J, Kingston BR, Maiorino L, Rothschild J, et al. The entry of nanoparticles into solid tumours. Nat Mater 2020;19:566–75.
9. Ali OA, Huebsch N, Cao L, Dranoff G, Mooney DJ. Infection-mimicking materials to program dendritic cells in situ. Nat Mater 2009;8:151–8.
10. Ali OA, Emerich D, Dranoff G, Mooney DJ. In situ regulation of DC subsets and T cells mediates tumor regression in mice. Sci Transl Med 2009;1:8ra19.
11. Li AW, Sobral MC, Badrinath S, Choi Y, Graveline A, Stafford AG, et al. A facile approach to enhance antigen response for personalized cancer vaccination. Nat Mater 2018;17:528–34.
12. Adu-Berchie K, Brockman JM, Liu Y, To TW, Zhang DKY, Najibi AJ, et al. Adoptive T cell transfer and host antigen-presenting cell recruitment with cryogel scaffolds promotes long-term protection against solid tumors. Nat Commun 2023;14:3546.
13. Bencherif SA, Warren SR, Ali OA, Li WA, Lewin SA, Braschler TM, et al. Injectable cryogel-based whole-cell cancer vaccines. Nat Commun 2015;6:7556.
14. Bhattacharya P, Budnick I, Singh M, Thiruppathi M, Alharshawi K, Elshabrawy H, et al. Dual role of GM-CSF as a pro-inflammatory and a regulatory cytokine: implications for immune therapy. J Interferon Cytokine Res 2015;35:585–99.
15. Kumar A, Taghi Khani A, Sanchez Ortiz A, Swaminathan S. GM-CSF: a double-edged sword in cancer immunotherapy. Front Immunol 2022;13:901277.
16. Hong I-S. Stimulatory versus suppressive effects of GM-CSF on tumor progression in multiple cancer types. Exp Mol Med 2016;48:e242.
17. van de Laar L, Coffer PJ, Woltman AM. Regulation of dendritic cell development by GM-CSF: molecular control and implications for immune homeostasis and therapy. Blood 2012;119:3383–93.
18. Cohen S, Yoshioka T, Lucarelli M, Hwang LH, Langer R. Controlled delivery systems for proteins based on poly(lactic/glycolic acid) microspheres. Pharm Res 1991;8:713–20.
19. Gentile P, Chiono V, Carmagnola I, Hatton PV. An overview of poly(lactic-co-glycolic) acid (PLGA)-Based biomaterials for bone tissue engineering. Int J Mol Sci 2014;15:3640–59.
20. Lü J-M, Wang X, Marin-Muller C, Wang H, Lin PH, Yao Q, et al. Current advances in research and clinical applications of PLGA-based nanotechnology. Expert Rev Mol Diagn 2009;9:325–41.
21. Carey CD, Gusenleitner D, Lipschitz M, Roemer MGM, Stack EC, Gjini E, et al. Topological analysis reveals a PD-L1-associated microenvironmental niche for Reed-Sternberg cells in Hodgkin lymphoma. Blood 2017;130:2420–30.
22. Patel SS, Weirather JL, Lipschitz M, Lako A, Chen P-H, Griffin GK, et al. The microenvironmental niche in classic Hodgkin lymphoma is enriched for CTLA-4–positive T cells that are PD-1–negative. Blood 2019;134:2059–69.
23. Thrash EM, Kleinsteuber K, Hathaway ES, Nazzaro M, Haas E, Hodi FS, et al. High-throughput mass cytometry staining for immunophenotyping clinical samples. STAR Protoc 2020;1:100055.
24. Kleinsteuber K, Corleis B, Rashidi N, Nchinda N, Lisanti A, Cho JL, et al. Standardization and quality control for high-dimensional mass cytometry studies of human samples. Cytometry A 2016;89:903–13.
25. Konopka T. Umap: uniform manifold approximation and projection. R Package Version 0.2.7.0. Available from: https://CRAN.R-project.org/package=umap.

26. Wickham H. ggplot2: elegant graphics for data analysis. In: Wickham H, editor. Ggplot2 Elegant Graph Data Anal [Internet]. New York (NY): Springer; 2016. [cited 2021 Oct 3]. Available from: 10.1007/978-0-387-98141-3_1.
27. Kolde R. pheatmap: pretty Heatmaps. R package version 1.0.12. 2019. Available from: https://CRAN.R-project.org/package=pheatmap.
28. Wang Y, Han G, Wang K, Liu G, Wang R, Xiao H, et al. Tumor-derived GM-CSF promotes inflammatory colon carcinogenesis via stimulating epithelial release of VEGF. Cancer Res 2014;74:716–26.
29. Mackey MF, Gunn JR, Ting PP, Kikutani H, Dranoff G, Noelle RJ, et al. Protective immunity induced by tumor vaccines requires interaction between CD40 and its ligand, CD154. Cancer Res 1997;57:2569–74.
30. Xu LL, McVicar DW, Ben-Baruch A, Kuhns DB, Johnston J, Oppenheim JJ, et al. Monocyte chemotactic protein-3 (MCP3) interacts with multiple leukocyte receptors: binding and signaling of MCP3 through shared as well as unique receptors on monocytes and neutrophils. Eur J Immunol 1995;25:2612–7.